

Journal of Fluid Mechanics

<http://journals.cambridge.org/FLM>

Additional services for *Journal of Fluid Mechanics*:

Email alerts: [Click here](#)

Subscriptions: [Click here](#)

Commercial reprints: [Click here](#)

Terms of use : [Click here](#)



Stratified separated flow around a mountain with an inversion layer below the mountain top

J. C. R. HUNT, G. G. VILENSKI and E. R. JOHNSON

Journal of Fluid Mechanics / Volume 556 / June 2006, pp 105 - 119

DOI: 10.1017/S0022112006009335, Published online: 24 May 2006

Link to this article: http://journals.cambridge.org/abstract_S0022112006009335

How to cite this article:

J. C. R. HUNT, G. G. VILENSKI and E. R. JOHNSON (2006). Stratified separated flow around a mountain with an inversion layer below the mountain top. Journal of Fluid Mechanics, 556, pp 105-119 doi:10.1017/S0022112006009335

Request Permissions : [Click here](#)

Stratified separated flow around a mountain with an inversion layer below the mountain top

By J. C. R. HUNT¹, G. G. VILENSKI² AND E. R. JOHNSON²

¹Centre for Polar Observations and Modelling, Department of Space and Climate Physics, and Department of Earth Sciences, Gower Street, London, WC1E 6BT, UK

²Department of Mathematics, University College London, Gower Street, London, WC1E 6BT, UK

(Received 23 August 2004 and in revised form 24 November 2005)

This paper presents analytical and numerical results for separated stratified inviscid flow over and around an isolated mountain in the limit of small Froude number. The vertical density profile consists of a lower strongly stratified layer whose depth is just less than that of the mountain. It is separated from a semi-infinite upper stably stratified layer by a thin, highly stable, inversion layer. The paper aims to provide, for this particular profile, a thorough analysis of the three-dimensional separated flow over a mountain top with strong stratification. The Froude numbers F and F_I of the lower layer and the interface are small with $F_I \ll F \ll 1$, but the upper-layer Froude number is arbitrary. The flow at each height in the lower layer is governed by the two-dimensional Euler equations and moves horizontally around the mountain. It is given by a modification of a previous model using Kirchhoff free-streamline theory for the separated flow region downstream of the mountain. The pressure variations associated with the lower-layer flow are of the same order as the dynamic head and induce significant displacements of the inversion layer. When the inversion is near the top of the mountain these deflections are of the same order as the height of the projecting part of the mountain top and combine with the flow over the mountain top to excite vertically propagating internal waves in the upper layer. The resultant pressure field, vertical stream surface displacements, and surface streamlines in the upper layer are described consistently in the hydrostatic limit. Many of the features of the upper flow, including the perturbations of the critical dividing streamlines, are similar to those in flows with uniform stable stratification at low Froude number. Comparisons are made with experiments and approximate models for these summit flows based on the assumption that the dividing streamlines have small vertical displacement.

1. Introduction

Three-dimensional flows over orography with strong stable upstream stratification have been extensively studied computationally (e.g. Smolarkiewicz & Rotunno 1989) and experimentally (e.g. Brighton 1978*a, b*; Lin *et al.* 1992; Vosper *et al.* 1999). However, two central questions remain unanswered, namely how the separated wake flow is affected by buoyancy forces and how it interacts with the flow over the mountain. Approximate models have been proposed both for the time mean and fluctuating structure of the wake (e.g. Chomaz, Bonneton & Hopfinger 1993; Hunt *et al.* 1997; Hunt & Fernando 1998), but no systematic theoretical model has been proposed covering all the related regions of the flow, even for steady flow over an idealized shape. The objective of this paper is to provide such a model for a particular shape and type of approach flow.

In these kinds of flow, around most high mountains and mountain ranges in the atmosphere and around many sea mounts in the ocean, the Froude number is usually small (≤ 0.3). The drag forces exerted by the obstacles and the flow perturbations produced by them have a large effect on the local and general circulation of the atmosphere and ocean. Even though Coriolis forces have a significant effect on the far field, the flow around an isolated mountain is dominated by inertial and buoyancy forces (e.g. Hunt, Olafsson & Bougeault 2001). For very large mountains, Coriolis forces and flow separated flow significantly alter the overall flow around the mountain itself (e.g. Orr *et al.* 2005). However, in most practical estimates for the drag of mountains used in numerical weather prediction codes, Coriolis forces are neglected (Lott & Miller 1997).

At sufficiently high Reynolds number with constant density gradient, stably stratified flows are characterized by the Froude number $F = U_\infty / NH$ based on the mountain height H , unperturbed flow velocity U_∞ and buoyancy frequency N . When a stable inversion layer with relative density jump $\Delta\rho/\rho$ is present near the summit of the mountain, the flow depends also on the Froude number of the inversion layer $F_I = U_\infty / \sqrt{g'H}$, where $g' = g\Delta\rho/\rho$. Laboratory experiments have broadly confirmed Drazin's (1961) steady-state theory that for $F \ll 1$ and $F_I = \infty$ (so no inversion layer is present), the bulk of the flow is quasi-two-dimensional in horizontal planes, except within thin layers, of thickness HF , at the top and bottom of a mountain (Sheppard 1956; Snyder, Britter & Hunt 1980; Greenslade 1994). According to Smolarkiewicz & Rotunno (1989) and Hunt *et al.* (1997), this is why vertical vorticity is present in the flow and why flow separation is driven by an essentially inviscid mechanism. In Drazin's inviscid analysis, the horizontal flow below the mountain top is not matched with the baroclinic flow over the top where significant vertical vorticity is generated. Also, in the top layer, the fluctuations are of order FH , producing waves that propagate downwards as well as upwards (Newley, Pearson & Hunt 1991). This explains why experimental results for vertical deflections are larger than the amplitude $O(F^2H)$ predicted by Drazin's theory (Hunt *et al.* 1997; Vosper *et al.* 1999).

Laboratory experiments (Snyder *et al.* 1980) have shown that the separated flow region has only a weak effect on flow near the top of the mountain. There was little difference in the flow over the top when it was isolated by fixing a flat horizontal plate at the level of the dividing streamline that separates the top layer from the two-dimensional bluff flow below. Here, the complex interaction between these regions is studied by analysing flow situations where a strongly stably stratified, arbitrarily thin inversion layer lies just below the top of the mountain. This is a common meteorological situation, as seen in satellite pictures of clouds around isolated mountains (Smolarkiewicz, Rasmussen & Clark 1988; Smith & Grubisic 1993; Smith *et al.* 1997), and for this particular stratification, the mathematical analysis of the thin layer near the top of the mountain is linear, which is not the case when there is no inversion layer (Greenslade 2000). The flow below the inversion, including the separated flow region, produces dynamic pressure perturbations and deflections of the inversion layer, which perturbs the flow above the inversion. However, when the inversion layer is strong, the upper flow does not affect the wake region or the flow in the lower layer.

The laboratory experiments of Brighton (1978*b*), Hunt *et al.* (1997) and Vosper *et al.* (1999) show that the wake in the main region is generally unsteady. For $F < 0.4$, flows are characterized by periodic vortex shedding with a Strouhal number $S = \omega L / U_\infty$ (for ω the frequency of vortex shedding and L the obstacle base width) of approximately 0.2 for a wide variety of body shapes. The position of the separation lines on the sides of the body oscillates periodically and varies with height. These unsteady effects are not treated here in detail because the unsteady velocity

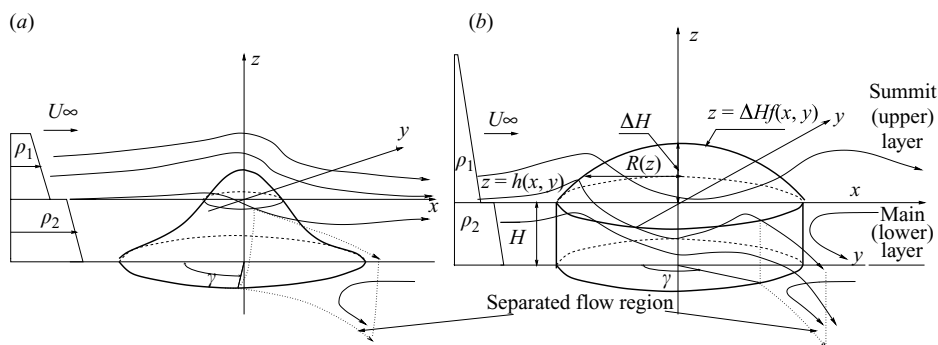


FIGURE 1. The form of stably stratified separated flow around an axisymmetric three-dimensional mountain at low Froude number. (a) A typical mountain with sloping sides. (b) The idealized mountain with a rounded top discussed here. Note the separation angle γ .

fluctuations (with pressure fluctuations of order $0.1\rho U_\infty^2$) produce only weak vertical fluctuating displacements of the inversion layer of order $0.1F_l^2H$. Because $F \ll 1$, these displacements produce weak waves which propagate approximately horizontally in the upper layer (Carruthers & Hunt 1986). The boundary-layer flow, vortex shedding and the pressure gradient in the lower layer all affect the mean separation position through the displacement of the inversion layer. Some studies of the wakes behind isolated mountains with vortex shedding and elevated inversion layers have indicated that they are similar to low-Reynolds-number wakes, with laminar-like separation positions. This may be associated with the mountain having very low slopes at the level of the inversion layer (Brighton, personal communication). Without inversion layers in flows at low Froude number (and order-one slope), the locations of the separation points are similar to those at high-Reynolds-number flow around bluff bodies (e.g. Hunt & Snyder 1980). In this paper, we consider a full range of separation positions.

Experiments and computations with bodies of different shapes (Sysoeva & Chashechkin 1988; Olafsson & Bougeault 1997; Vosper *et al.* 1999) show that the mean wake profiles immediately behind the obstacles differ significantly depending on the type of body and the Froude number. A physical argument in Hunt & Fernando (1998), based on idealized experiments with sloping vortices, and the experiments of Sysoeva & Chashechkin (1988) suggest that sufficiently far downstream from the obstacle, the wake becomes approximately rectangular. To avoid some of the special features of wakes of sloping mountains, the mountain in the analysis here is chosen to be cylindrical below the inversion layer with a rounded top above the inversion. For this geometry, the flow is taken to separate in the lower layer, but remains attached above the inversion (figure 1). This ensures that the form of the flow is similar to those of the experimental results of Brighton (1978*a, b*); Hunt & Snyder (1980) and the numerical study by Hanazaki (1994) of rounded obstacles showing that the flow separates below the summit region. Section 2 gives further details of the flow configuration. Section 3 describes the lower-layer flow and §4 the flow aloft. Section 5 briefly discusses the results.

2. Flow configuration and governing equations

Consider the steady flow of two stably stratified fluid layers separated by a very thin, strongly stably stratified inversion layer past an obstacle of typical horizontal scale L

(figure 1). The aim is to calculate the flow fields above and below the inversion which are coupled because of the vertical deflection of the layer. The effects of the strengths of the stable stratification in the two layers in relation to that of the inversion layer and the difference in level between the inversion layer and the top of the hill are analysed in detail. It is assumed that the Reynolds number is large and that the height of the hill above the inversion layer is sufficiently small that in the flow over the hill above the inversion layer there is no separation. Take Cartesian axes $Ox^*y^*z^*$ so that Oz^* is the vertical (upwards positive) axis of symmetry of the obstacle, the plane $z^* = 0$ coincides with the undisturbed inversion layer far from the obstacle, and Ox^* is in the direction of the flow at large distance, which is taken to be uniform of speed U_∞ . Let the undisturbed density profiles in the two layers be $\rho_{i\infty}(z^*)$ (here, and elsewhere, $i = 1, 2$ corresponding to the upper and lower layers, respectively), so that the density jump across the inversion is $\Delta\rho = \rho_{2\infty}(0) - \rho_{1\infty}(0) = \rho_{2\infty}(0)(1 - \kappa) > 0$, for $\kappa = \rho_{1\infty}(0)/\rho_{2\infty}(0) < 1$. In order to focus on the effects of the inversion layer, it is assumed that in both the upper and lower layers, the stratification is uniform and has the same strength (defined by the buoyancy frequency N). It is subsequently noted in §§3 and 4 and that this restriction is not necessary in the limit considered here. The obstacle stands on a flat bottom, $z = -H$, pierces the inversion layer and projects into the upper layer which is taken to be vertically unbounded. The non-dimensional velocity components (u_i, v_i, w_i) , perturbation densities ρ_i and pressures p_i , are formed from the corresponding (starred) dimensional quantities through the scalings

$$\left. \begin{aligned} (x^*, y^*, z^*) &= (Lx, Ly, Hz), & (u_i^*, v_i^*, w_i^*) &= U_\infty(u_i, v_i, Hw_i/L), \\ \rho_i^* &= \rho_{i\infty}(0) \left(1 - \frac{N^2 H}{g} (z - \rho_i) \right), & p_i^* &= \rho_{i\infty}(0) g H \left(-z + \frac{N^2 H}{2g} z^2 + \frac{U_\infty^2 p_i}{gH} \right), \end{aligned} \right\} \quad (2.1)$$

Since constant buoyancy frequency implies a linear density gradient (outside the inversion layer), the non-dimensional perturbation densities ρ_i have been scaled as non-dimensional vertical heights – the local vertical displacements of isopycnal surfaces from their upstream heights. The equations of motion in both layers can then be written (Baines 1995) as

$$(1 - (z - \rho_i)\beta^{-2})(u_i\partial_x + v_i\partial_y + w_i\partial_z) \begin{pmatrix} u_i \\ v_i \\ \varepsilon^2 w_i \end{pmatrix} + \begin{pmatrix} \partial_x p_i \\ \partial_y p_i \\ \partial_z p_i \end{pmatrix} + \begin{pmatrix} 0 \\ 0 \\ \rho_i/F^2 \end{pmatrix} = 0, \quad (2.2)$$

$$\partial_x u_i + \partial_y v_i + \partial_z w_i = 0, \quad (2.3)$$

$$(u_i\partial_x + v_i\partial_y + w_i\partial_z)\rho_i = w_i, \quad (2.4)$$

where

$$\varepsilon = \frac{H}{L}, \quad F_I = \frac{U_\infty}{\sqrt{g'H}}, \quad F = \frac{U_\infty}{NH}, \quad \beta = (1 - \kappa)^{-1/2} F/F_I = \sqrt{\frac{g}{N^2 H}}, \quad (2.5)$$

g is the acceleration due to gravity and $g' = g(1 - \kappa)$ is the reduced gravity at the interface.

Away from the obstacle, the kinematic condition on the two layers is that the inversion layer is very thin so the interface, $z = h(x, y)$, is a material surface and further that the pressure is continuous across the interface (e.g. Batchelor 1967). This

gives the matching conditions at $z = h(x, y)$,

$$w_i = u_i h_x + v_i h_y \quad (i = 1, 2), \quad (2.6)$$

$$\kappa p_1 - p_2 = -\bar{h}/\delta + (1 - \kappa)\bar{h}^2/2, \quad (2.7)$$

where $\bar{h} = h/F$ and $\delta = F_1^2/F$ is the ratio of the square of the Froude number of the inversion layer F_1 to the Froude number for the lower-layer flow F . Since the obstacle is impermeable, this provides a local kinematic condition,

$$w_i = u_i f_x + v_i f_y, \quad i = 1, 2 \quad \text{on } z = f(x, y). \quad (2.8)$$

Previous studies (Hunt *et al.* 1997; Greenslade 2000) have shown that if the obstacle projects a height $O(FH)$ above the dividing streamline then the flow in the upper layer is nonlinear with breaking internal waves and separated flow. Here, the height of the obstacle above the inversion layer is taken to be much less than $O(FH)$, given by

$$z = \alpha F \tilde{f}(x, y), \quad (2.9)$$

where \tilde{f} has maximum unity and $\alpha \ll 1$. Thus, the top of the mountain protrudes a height $\Delta H = \alpha FH$ above the inversion layer, and the flow perturbation in the upper layer is small.

The remaining vertical boundary condition on the semi-infinite upper layer is the radiation condition that there is no incoming energy from $z \gg 1$. In this non-dimensionalization, the uniform condition at large x, y becomes

$$h \rightarrow 0 \quad \rho_i \rightarrow 0, \quad (u_i, v_i, w_i) \rightarrow (1, 0, 0) \quad \text{as } x \rightarrow -\infty \quad (i = 1, 2). \quad (2.10)$$

The next step is to analyse the system (2.2)–(2.10) in the limit $F \rightarrow 0$, $\delta \rightarrow 0$ and $\alpha \rightarrow 0$ with $\sigma = \delta/\alpha$, ε and κ fixed. The small value of F means that Drazin's solution gives the leading-order flow in the lower layer (see §3). The small value of $\delta = F_1^2/F = U_\infty N/g'$ implies that inertial accelerations in the lower layer are much smaller than the reduced gravity at the interface. Thus, the highly stable inversion layer is only weakly distorted by the pressure field of the lower layer. The small values of α and δ mean that the orographically forced flow in the upper layer is only a linear perturbation of the approach flow. The ratio σ can be written as $\sigma = \delta/\alpha = F_1^2 H/\Delta H$. Thus, σ measures the relative importance of upper-layer interface displacements forced by the lower-layer pressure field compared to displacements forced by flow over orography. When $\sigma \ll 1$, the inversion layer remains flat and only the orography above the inversion layer affects the upper flow. As σ increases, the effect of the lower-layer forcing becomes significant, as shown in §4. Note that if both α and δ are of order unity, the upper-layer flow is fully nonlinear and three-dimensional and thus analytically intractable (Greenslade 1994).

3. The lower-layer flow

In the main part of the lower layer, the flow is horizontal to leading order. There is a small vertical velocity of order F^n , with $n \geq 1$ (see below), so, following Drazin (1961) and Brighton (1978*a, b*)

$$\left. \begin{aligned} u_2 &= u_0(x, y, z) + o(1), \\ v_2 &= v_0(x, y, z) + o(1), \\ w_2 &= F^n w_0(x, y, z) + o(F^n), \\ \rho_2 &= F^n \rho_0(x, y, z) + o(F^n), \\ p_2 &= p_0(x, y, z) + o(1). \end{aligned} \right\} \quad (3.1)$$

Substituting (3.1) into (2.2)–(2.10) gives the quasi-two-dimensional system for the horizontal velocity field

$$\left. \begin{aligned} (u_0 \partial_x + v_0 \partial_y) \begin{pmatrix} u_0 \\ v_0 \end{pmatrix} &= - \begin{pmatrix} p_{0x} \\ p_{0y} \end{pmatrix}, \\ p_{0z} &= -\rho_0, \quad w_0 = (u_0 \partial_x + v_0 \partial_y) \rho_0. \end{aligned} \right\} \quad (3.2)$$

with

$$u_0 f_x + v_0 f_y = 0 \quad \text{on } z = f(x, y), \quad (3.3)$$

$$(u_0, v_0, \rho_0) \rightarrow (1, 0, 0) \quad \text{as } x \rightarrow -\infty. \quad (3.4)$$

For axisymmetric obstacles, centred on $(x, y) = (1, 0)$, the shape $z = f(x, y)$ can be re-expressed as the obstacle radius $R(z)$ at each height z . If the flow remains attached to the body then (provided $dR/dz \ll O(F^2)$, Brighton 1978*a, b*) system (3.2)–(3.3) admits the leading-order Drazin solution which in each plane $z = \text{const}$ corresponds to two-dimensional irrotational flow about a circle of radius $R(z)$. A consistent solution for the vertical velocity perturbation in the expansion (3.1) was obtained by Drazin (1961) and Brighton (1978*a, b*), in which $n = 2$, but these solutions did not include the effects of vertical perturbations of order F which can propagate upward from the bottom and downward from the top of the obstacle where expansion (3.1) does not hold (Newley *et al.* 1991; Vosper *et al.* 1999). For the idealized case considered here by taking the obstacle to be a right circular cylinder of radius L (or unity when normalized), $R(z) \equiv 1$ and $w_0 = 0$. The largest vertical perturbation is then caused by the vertical displacement of the interface and is $O(F_I)$, much less than $O(F)$.

The main limitation of Drazin's theory is that it does not allow for the separated wake which always occurs in high-Reynolds-number flows. Therefore, here, the theory is extended to give a consistent model with a recirculating region downstream of the orography. As in Drazin's analysis, the stratification N is sufficiently strong and velocities are sufficiently small that vertical displacements remain negligible and system (3.2)–(3.3) remains valid. However, unlike Drazin's analysis, two free streamlines separate symmetrically (with respect to the flow centreline) from the surface of the cylinder in each horizontal plane. Within the separated region, the flow is stagnant and the pressure is the constant unperturbed far-field pressure. Along the free streamlines, the flow speed is U_∞ and once the points of separation of the free streamlines are fixed, the flow field in each horizontal plane follows from Kirchhoff free streamline theory (Brodetsky 1923; Birkhoff & Zarantonello 1957; Gurevitch 1965). In the context of the present purely inviscid theory, consistent separated solutions exist for a range of positions of the separation points. The precise position of the separation points in a given flow depends on a number of factors and thus solutions are presented here for the whole range of separation angles. Figure 2 shows pressure contours (isobars) in the (x, y) -plane for separation point positions corresponding to the three separation angles (measured from the forward stagnation point), $\gamma_S = 55^\circ 2' 15''$, 110° and 124° . The smallest angle, $\gamma_S = 55^\circ 2' 15''$, corresponds to smooth separation with the curvature of the free streamline being the same as the curvature of the rigid wall at separation. This is the classical Brillouin–Villat condition and is consistent with laminar boundary theory (Sychev 1972; Smith 1978). The largest angle, $\gamma_S = 124^\circ$, is close to the maximum permissible value of separation angle of $124^\circ 12' 34''$ when the free streamlines converge far downstream (Gurevitch 1965) and $\gamma_S = 110^\circ$ shows typical intermediate behaviour.

Experiments show that in high-Reynolds-number flows, the separation angle is unsteady and its mean value differs significantly between laminar and turbulent

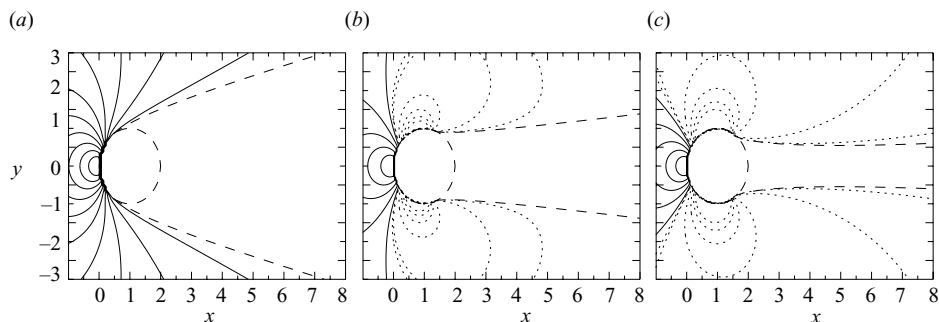


FIGURE 2. Pressure contours (isobars) in horizontal planes for separated Kirchhoff flow past a circular cylinder of unit radius for three separation angles (a) $\gamma = 55^\circ 21' 15''$, (b) $\gamma = 110^\circ$, (c) $\gamma = 124^\circ$. The cylinder and free streamlines are shown by long dashed lines. Positive pressure contours are shown in solid lines, negative pressure contours are short dashed lines.

flows. On mountains with small slopes (less than 0.1, say) the diffusion of vertical vorticity is large and even at high Reynolds number (based on mountain width and oncoming flow speed) the wake behaves more like a moderate Reynolds flow, as noted in the description of wakes behind Madeira by Moll (1971), summarized in Berger & Wille (1972). In this flow, figure 2(a) would be more relevant. For typical turbulent boundary layers, Gurevitch (1965) estimates the separation angle for steep topography to lie in the range $\gamma \simeq 120^\circ$ – 124° and then figure 2(c) is more relevant. Provided the separation angle is not too close to the maximum value, the separated wake region grows downstream like those described in the experimental work of Hunt & Snyder (1980). Flows past steep orography are most likely to resemble figure 2(c) (e.g. Smolarkiewicz & Rotunno 1989; Hunt *et al.* 1997).

4. The upper-layer flow

For small δ and α , the upper-layer flow is simply the linear internal wave field forced by the small perturbations at its lower boundary and so it can, in principle, be calculated for arbitrary profiles of stratification in the upper layer. Since here the upper-layer stratification has been taken to be the same as that in the lower layer, the vertical scale of wave motions is small, of order F . The stretched vertical variable $\zeta = z/F$, so ζ is of order unity in a layer of thickness F . Then system (2.2)–(2.10) admits a solution, linearized about undisturbed flow, of form

$$\left. \begin{aligned} u_1 &= 1 + \alpha u'(x, y, \zeta) + o(\alpha), \\ v_1 &= \alpha v'(x, y, \zeta) + o(\alpha), \\ w_1 &= \alpha F w'(x, y, \zeta) + o(\alpha F), \\ \rho_1 &= \alpha F \rho'(x, y, \zeta) + o(\alpha F), \\ p_1 &= \alpha p'(x, y, \zeta) + o(\alpha), \\ h &= \delta F h'(x, y, \zeta) + o(\alpha F), \end{aligned} \right\} \quad (4.1)$$

satisfying

$$\left. \begin{aligned} u'_x &= -p'_x, \quad v'_x = -p'_y, \quad \rho' = -p'_\zeta, \\ u'_x + v'_y + w'_\zeta &= 0, \quad \rho'_x = w. \end{aligned} \right\} \quad (4.2)$$

The flow is unperturbed at large horizontal distances so $(u', v', \rho') \rightarrow (0, 0, 0)$ as $x \rightarrow -\infty$ and the upper boundary condition for the layer is the requirement that the group velocity of radiated waves has a positive upwards component. The lower boundary

condition introduces the interaction with the lower layer. Since $\alpha \ll 1$, the linearized impermeability condition on the obstacle can be applied on $\zeta = 0$ (e.g. Smith 1980) so

$$w' = \tilde{f}_x(x, y) \text{ on } \zeta = 0 \text{ when } (x-1)^2 + y^2 < 1. \quad (4.3)$$

The new feature of the solution is that the vertical velocity is also forced by vertical movement on the interface. Thus,

$$w' = \sigma h'_x(x, y) \text{ on } \zeta = 0 \text{ when } (x-1)^2 + y^2 > 1. \quad (4.4)$$

The interface displacement is determined from the lower-layer pressure through (2.7). Since p_1 is of order $\alpha \ll 1$ and $\bar{h} = h/F$ is of order $\delta \ll 1$, only two terms of (2.7) contribute at leading order, giving

$$h' = p_0(x, y, 0) \text{ on } \zeta = 0 \text{ when } (x-1)^2 + y^2 > 1, \quad (4.5)$$

with the interface displacement determined by the lower-layer pressure field. Because $\alpha \ll 1$, the pressure fluctuations produced by the flow in the upper layer, of order α , are much weaker than those produced by the lower layer and so the pressure contours of the lower-layer separated Kirchhoff flow determine the contours of the interface elevation.

The results for the laminar flow separation angle in figure 2(a) show that p_0 and h attain their maximum values at the forward stagnation point and then gradually decrease downstream. For turbulent flow separation, figure 2(c) shows the same deflection around the stagnation point, but a marked dip in the pressure and inversion height at the sides of the mountain, just upstream of the separation point. Downstream of separation the displacement decreases to zero.

System (4.2)–(4.5) reduces to the linear hydrostatic internal wave equation for the density fluctuations, namely

$$\rho'_{xx} + \rho'_{yy} + \rho'_{xx\zeta\zeta} = 0, \quad (4.6)$$

with boundary conditions

$$\rho'(x, y, \zeta = 0) = \tilde{h}(x, y) = \begin{cases} \sigma h'(x, y) & \text{for } (x-1)^2 + y^2 > 1, \\ \tilde{f}(x, y) & \text{otherwise.} \end{cases} \quad (4.7)$$

The solution of (4.6)–(4.7) subject to the radiation condition has the straightforward Fourier transform expression (Smith 1980)

$$\rho'(x, y, \zeta) = \left(\frac{1}{2\pi}\right)^2 \iint_{-\infty}^{+\infty} \hat{h}(k, l) \exp\left(i\left[\zeta \frac{\sqrt{k^2 + l^2}}{k} + kx + ly\right]\right) dk dl, \quad (4.8)$$

where $\hat{h}(k, l) = \iint_{-\infty}^{+\infty} \tilde{h}(x, y) \exp(-i[kx + ly]) dx dy$. In the numerical solutions below, the obstacle shape in the upper layer is paraboloidal with

$$\tilde{f}(x, y) = 1 - (x-1)^2 - y^2 \quad \text{for } (x-1)^2 + y^2 < 1. \quad (4.9)$$

Figure 3(a) shows the density field above the obstacle for $\sigma = 0$ when the inversion layer is so strong that the lower-layer pressure field cannot perturb it and it remains horizontal. The density field is then precisely that for flow over an axisymmetric obstacle on a flat plane. The flow is closely similar to the hydrostatic stratified flow over a bell-shaped mountain described by Smith (1980). However, the discontinuity in the slope of the streamlines where the obstacle intersects the inversion level introduces small perturbations downstream of the obstacle that are not present behind smooth

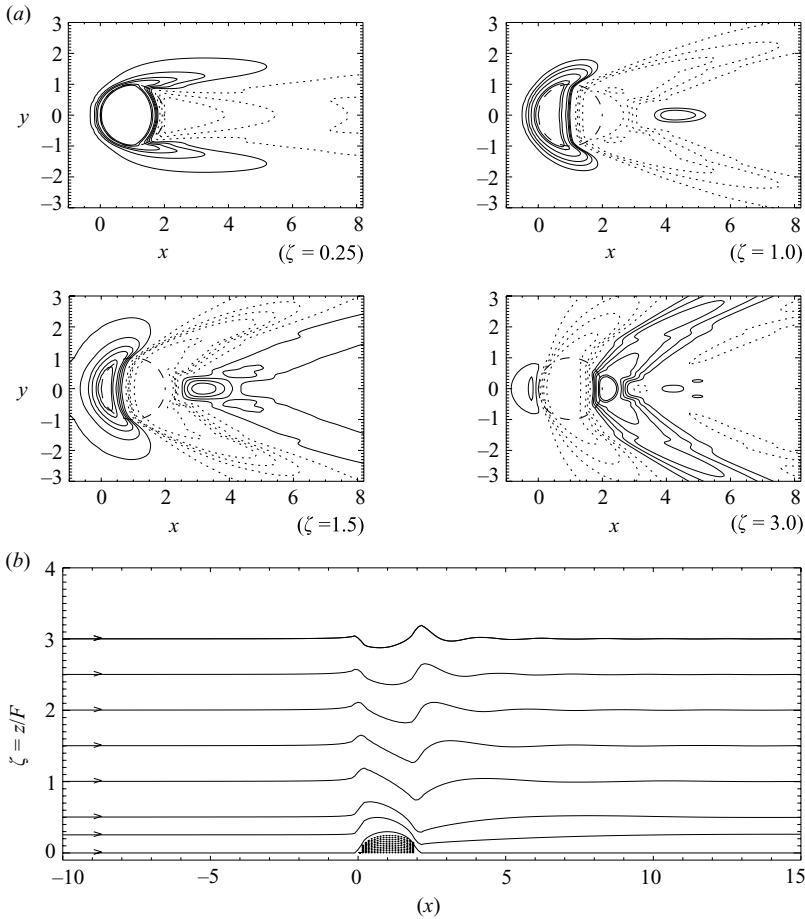


FIGURE 3. (a) Contours of the density perturbation $\rho' = \rho_1/(\alpha F)$ at different levels $\zeta = z/F$ for the paraboloidal obstacle (2.9), (4.9) when $\sigma = 0$ when the inversion layer is so strong that it remains flat. The obstacle perimeter is shown with a long dashed line. Solid lines correspond to positive ρ' (upward displacements of upstream level surfaces), dashed lines to negative ρ' (downward displacements). (b) Streamlines, or lines of constant density perturbation ρ_1/F , along the plane of symmetry $y=0$ for different values of ζ and $\alpha=0.3$. Each plot is shifted vertically by its value of ζ . The flow is from left to right.

topography (Feng 1995). These perturbations also appear in figure 3(b) which shows normalized density perturbation profiles ρ_1/F as functions of x in the plane of symmetry $y=0$ for different values of ζ . The slope discontinuity causes density profiles to steepen near the rear of the obstacle.

When σ is finite but still small (i.e. $\sigma < 1$), the wave pattern in the upper layer continues to be mainly determined by the projecting part of the obstacle rather than by the separation in the lower layer. Figure 4 shows the density contours for $\sigma = 0.5$ and for two separation angles, $\gamma_S = 55^\circ 2' 15''$ and $\gamma_S = 124$. The higher pressure associated with flow deceleration in the lower layer causes upward displacements of the stream surfaces near the interface in the upper fluid with the streamwise extent of the regions of positive perturbations near the obstacle decreasing with height. The downstream shift of the separation point in moving from figures 4(a) to 4(b) introduces density perturbations somewhat upstream of the separation point and in

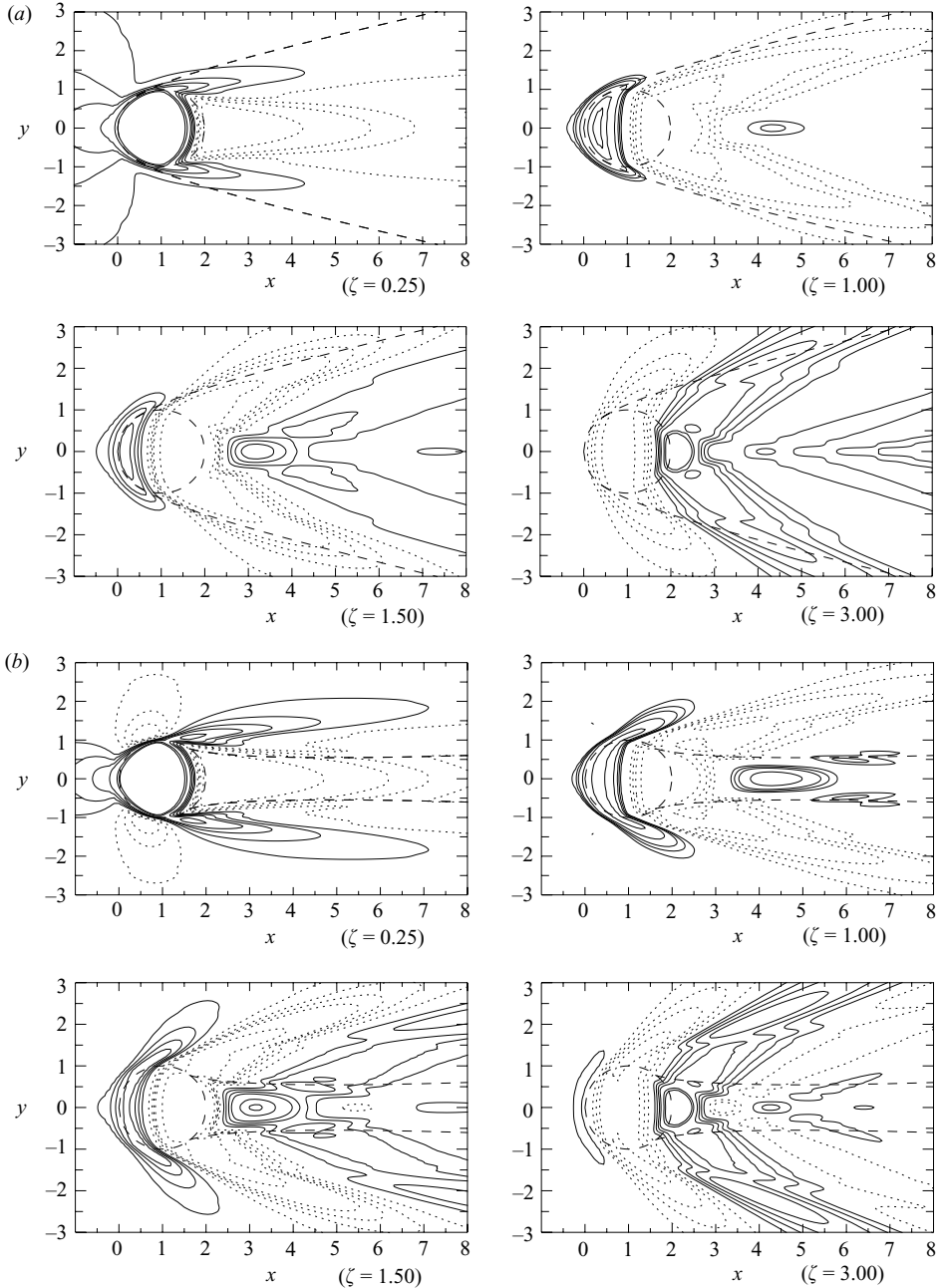


FIGURE 4. Density perturbation contours $\rho' = \rho_1/(\alpha F)$ at different levels above the inversion layer ($\zeta = 0.25, 1.0, 1.5, 3.0$) as in figure 3(a) but for $\sigma = 0.5$ (weak perturbation of the inversion layer). The lower-layer separation angles are (a): $\gamma_S = 55^\circ 2' 15''$ and (b): $\gamma_S = 124^\circ$. The dashed lines behind the obstacle show the positions of the two free streamlines in the lower layer.

the wake region. These tend to become V-shaped at higher levels above the mountain where they have crests and troughs along the line of symmetry (as in figure 4b, $\zeta = 3.0$). This is not typical of hydrostatic flow and has been previously attributed to non-hydrostatic effects (Smith 1980).

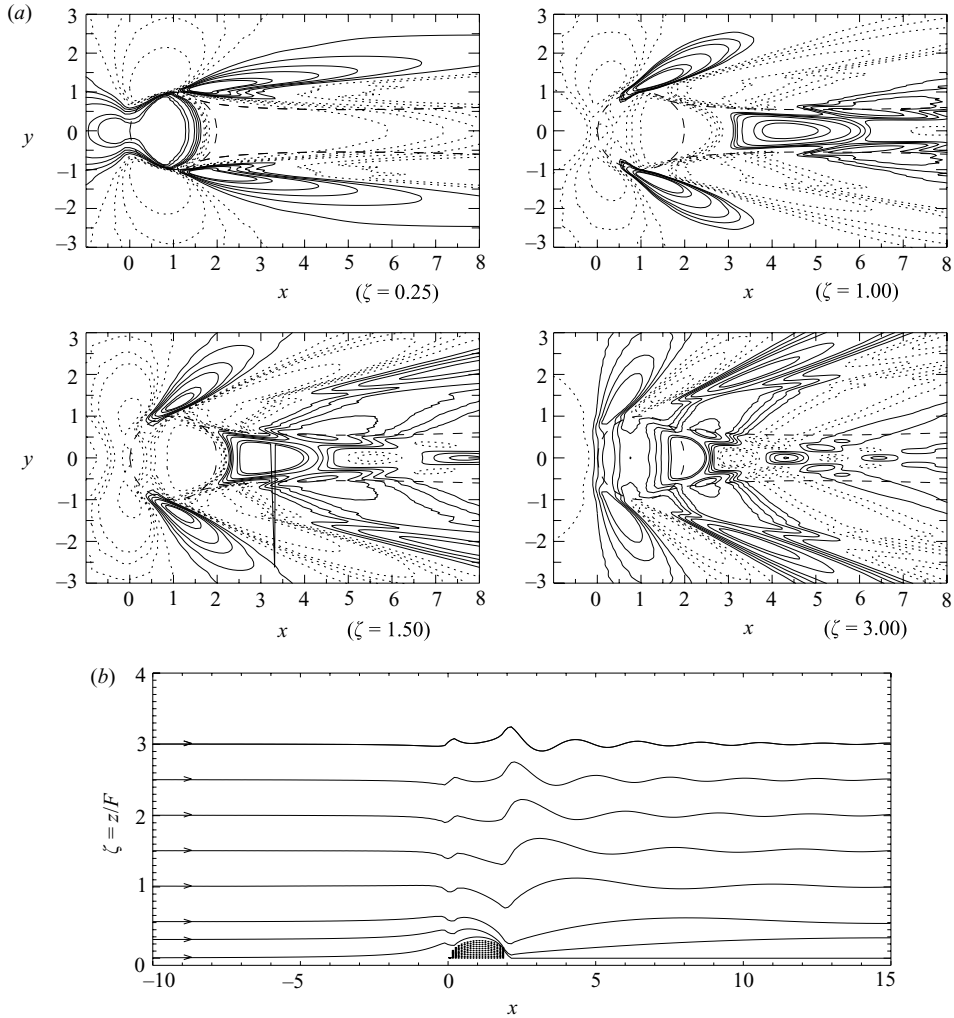


FIGURE 5. (a) Density perturbation contours $\rho' = \rho_1/(\alpha F)$ at different heights ζ as in figure 4, but for higher Froude number $\sigma = 1.5$ and $\gamma_S = 124^\circ$. (b) Streamlines, or constant density perturbation contours ρ_1/F for this flow with $\alpha = 0.3$ as in figure 3(a).

For $\sigma > 1$, lower-layer pressure distribution and the consequent vertical displacement of the inversion layer affects the upper-layer wave field. Since the separation of the flow in the lower-layer has such a large effect on the pressure distribution downstream of the obstacle, it significantly influences the wave pattern. This appears clearly in figure 5(a) which shows density contours in horizontal planes and in figure 5(b) which shows streamlines or density perturbation profiles in the plane of symmetry $y=0$ for $\sigma = 1.5$. The main feature of the flow around the mountain is the strong density perturbation near the separation region. Note in figures 3(b) and 5(b) how, as the Froude number rises, the flow over the obstacle in the upper-layer becomes asymmetric. There is a strong lee side downflow, even when $F \ll 1$, which leads to a deflection of the inversion layer (or dividing streamline) on the lee side (Hunt & Snyder 1980; Orr *et al.* 2005). The amplitude of the downstream wavetrain far above the mountain is also larger than for $\sigma = 0.5$.

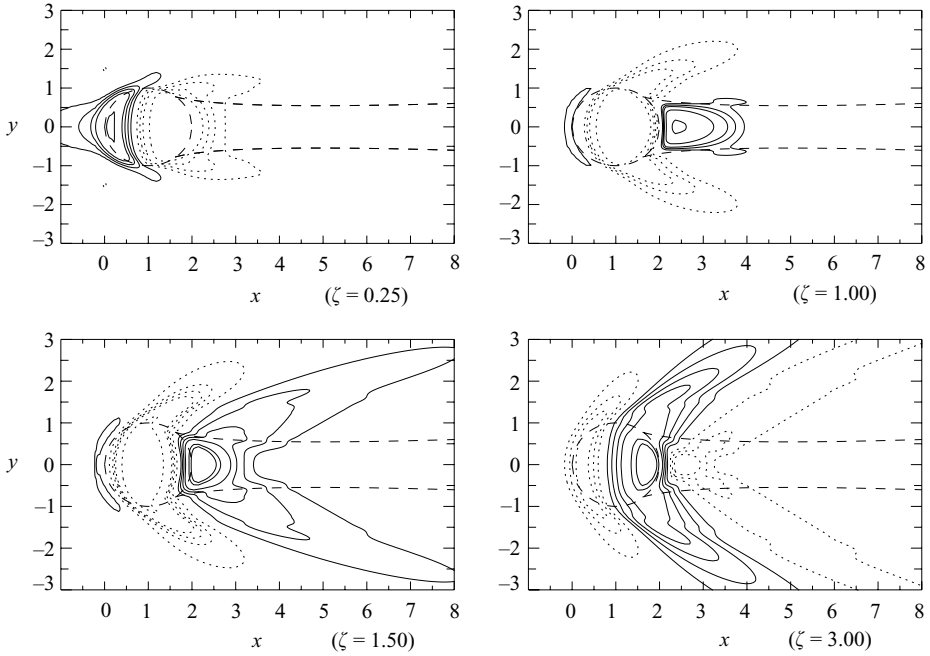


FIGURE 6. Contours of the upper-layer pressure perturbation $p' = p_1/\alpha$ at different heights ζ for $\sigma = 0.5$ $\gamma = 124^\circ$. Solid lines correspond to positive p' and dashed to negative p' .

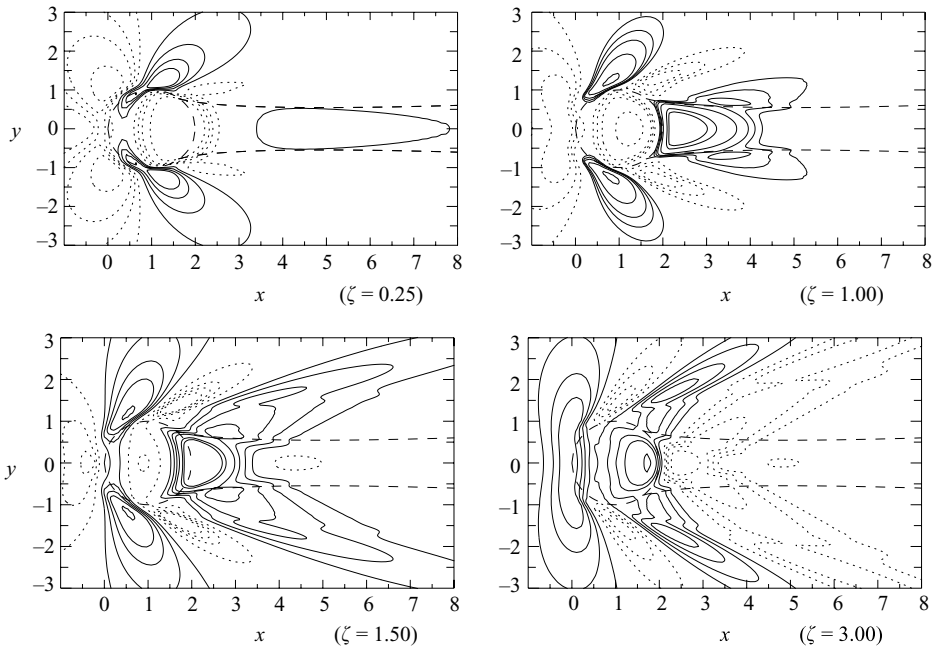


FIGURE 7. Contours of the upper-layer pressure perturbation $p' = p_1/\alpha$ as in figure 6, but for $\sigma = 1.5$.

Figures 6 and 7 give the pressure perturbation contours corresponding to figures 4 and 5. The pressure fields mimic the corresponding density fields and show a dispersive V-shaped wave pattern developing behind the obstacle with increasing height. The

increase in σ between figures 6 and 7 increases the relative importance of the lower-layer pressure field and intensifies the V-wave above the summit and wake, and produces stronger waves in the symmetry plane $y=0$. Figure 7 shows that, for large σ , the lower-layer pressure forces positive pressure perturbations in the upper layer on each side of the obstacle somewhat upstream of the separation points. With increasing height, these regions grow until they eventually merge above the front of the obstacle. For small σ , figure 6 shows that these side regions are not present and with increasing height, ζ , a region of negative pressure forms above the front of obstacle.

5. Conclusions

The idealized model here for two-layer strongly stratified steady flow over an obstacle illustrates the main effects of flow separation below the summit layer on the flow in this layer and over the top of the mountain. The flow in the upper layer is controlled by $\sigma = \delta/\alpha$, the ratio of $\delta FH = U_\infty^2/g'$, the height of interface perturbations forced by dynamic pressure variations in the lower layer, to $\Delta H = \alpha FH$, the height of the obstacle projecting into the upper layer. For small σ , the interface is effectively rigid, the flow over the summit is effectively that of flow over an obstacle on a flat plate, and lower-layer flow separation has no effect in the upper layer. For $\sigma > 1$, lower-layer separation strongly interacts with the upper-layer flow, in particular, affecting the wave field aloft through a substantial downward deflection of the interface somewhat upstream of the separated region. This deflection introduces changes in the density and pressure perturbations in the summit flow with magnitudes comparable to those in flow over a ‘cutoff’ mountain (the case $\sigma = 0$). Pressure distributions for large σ thus differ significantly from those for small σ . The wave pattern, similar to non-hydrostatic periodic linear lee waves, which develops downstream of the obstacle above the separation region is also of higher amplitudes when $\sigma > 1$ than when $\sigma < 1$.

Increasing the separation angle γ_S increases flow perturbations in the summit flow, and especially in the downstream wake region. Perturbations in turbulent flows can thus be expected to be bigger than in laminar flows even when velocities within the separation region are close to zero. The interface displacement is downward for the smaller (laminar) separation angle $\gamma \approx 55^\circ$. This agrees qualitatively with the experimental observations of Hunt & Snyder (1980) for $F=0.2$ and Vosper *et al.* (1999) for $F < 0.4$, although comparisons between the experiments and the present theory can only be qualitative owing to the different flow set-up. For larger (turbulent) angles when $\gamma > 55^\circ$, the interface is initially displaced downwards in front of the body, but then recovers near the separated region. The amplitude of the displacement is of order U_∞^2/g' and depends only on the strength of the inversion layer. This can be compared with the amplitude U_∞/N , of the vertical displacement for uniformly stratified flow (without an inversion). The summit flow, in these two types of stratified flow are similar if the buoyancy change of the inversion layer, g' , is of the same order as the buoyancy change, of order FHN^2 , in the summit layer for the uniformly stratified flow as $U_\infty^2/g' \sim U_\infty^2/FHN^2 \sim U_\infty/N$.

Although the numerical results have been presented here for strong stratification in the upper layer, the flow is governed there by the linear internal wave equation and so results for weak or non-uniform stratification, or for a finite-height upper layer, follow immediately. A significant extension of the present analysis would be the inclusion of Coriolis effects to describe separated flow around large mountain plateaux such as Greenland (Orr *et al.* 2005).

This work was supported by the UK Natural Environment Research Council under Grant NER/A/S/2000/01323. We are grateful for useful conversations with Professor

I. Castro and H. Olafsson. J.C.R.H. is grateful for support from Cornell University, where he is Mary B. Upson visiting professor, and E.R.J. is grateful to the School of Mathematical Sciences at Monash University, where he is a Research Associate, for their continued support and hospitality.

REFERENCES

- BAINES, P. G. 1995 *Topographic Effects in Stratified Flows*. Cambridge University Press.
- BATCHELOR, G. K. 1967 *An Introduction to Fluid Dynamics*. Cambridge University Press.
- BERGER, E. & WILLE, R. 1972 Periodic flow phenomena. *Annu. Rev. Fluid Mech.* **4**, 313–338.
- BIRKHOFF, G. & ZARANTONELLO, E. H. 1957 *Jets, Wakes and Cavities*. Academic.
- BRIGHTON, P. 1978a Boundary layer and stratified flows past obstacles. PhD thesis, University of Cambridge.
- BRIGHTON, P. W. M. 1978b Strongly stratified flow past 3-dimensional obstacles. *Q. J. R. Met. Soc.* **104**, 289–307.
- BRODETSKY, S. 1923 Discontinuous fluid motion past circular and elliptic cylinders. *Proc. R. Soc. A* **102**, 542–553.
- CARRUTHERS, D. J. & HUNT, J. C. R. 1986 Velocity fluctuations near an interface between a turbulent region and a stably stratified layer. *J. Fluid Mech.* **165**, 475–501.
- CHOMAZ, J., BONNETON, J. M. & HOPFINGER, E. 1993 The structure of the near wake moving horizontally in a stratified flow. *J. Fluid Mech.* **254**, 1–21.
- DRAZIN, P. G. 1961 On the steady flow of a fluid of variable density past an obstacle. *Tellus* **13**, 239–251.
- FENG, Y. 1995 Stably stratified shear flow over complex terrain. PhD thesis, University of Cambridge.
- GREENSLADE, M. D. 1994 Strongly stratified airflow over and around mountains. In *Stably Stratified Flows: Flow and Dispersion over Topography* (ed. I. P. Castro & N. J. Rockcliff). Oxford.
- GREENSLADE, M. D. 2000 Drag on a sphere moving horizontally in a stratified fluid. *J. Fluid Mech.* **418**, 339–550.
- GUREVITCH, M. L. 1965 *Theory of Jets in Ideal Fluids*. Academic.
- HANAZAKI, H. 1994 On the three-dimensional internal waves excited by topography in the flow of a stratified fluid. *J. Fluid Mech.* **263**, 293–318.
- HUNT, J. C. R., FENG, Y., LINDEN, P. F., GREENSLADE, M. D. & MOBBS, S. D. 1997 Low-Froude-number stable flows past mountains. *Nuovo Cimento Soc. Ital. Fis. C-Geophys. Space Phys.* **20**, 261–272.
- HUNT, J. C. R. & FERNANDO, H. J. S. 1998 Separated flow around bluff obstacles at low Froude number: vortex shedding and estimates of drag. In *Proc. 5th IMA Conf. on Stably Stratified Flows, Dundee, 1996* (ed. P. Davies). Clarendon.
- HUNT, J. C. R., OLAFSSON, H. & BOUGEALT, P. 2001 Coriolis effects on orographic and mesoscale flows. *Q. J. R. Met. Soc.* **127**, 601–633.
- HUNT, J. C. R. & SNYDER, W. H. 1980 Experiments on stably and neutrally stratified flow over a model three-dimensional hill. *J. Fluid Mech.* **9**, 671–704.
- LIN, Q., LINBERG, W. R., BOYER, D. L. & FERNANDO, H. J. S. 1992 Stratified flow past a sphere. *J. Fluid Mech.* **240**, 315–354.
- LOTT, F. & MILLER, M. J. 1997 A new subgrid-scale orographic drag parametrization: its formulation and testing. *Q. J. R. Met. Soc.* **123**, 101–127.
- MOLL, H. G. 1971 Die atmosphärische Umströmung Madeiras. *Beitr. Z. Phys. Atmos.* **44**, 102–118.
- NEWLEY, T. M. J., PEARSON, H. J. & HUNT, J. C. R. 1991 Stably stratified rotating flow through a group of obstacles. *Geophys. Astrophys. Fluid Dyn.* **58**, 147–171.
- OLAFSSON, H. & BOUGEALT, P. 1997 The effect of rotation and surface friction on orographic drag. *J. Atmos. Sci.* **54**, 193–210.
- ORR, A., HANNA, E., HUNT, J. C. R., CAPPELEN, J., STEFEN, K. & STEPHENS, A. G. 2005 Characteristics of stable flows over southern Greenland. *Pure Appl. Geophys.* **162**, 1747–1778.
- SHEPPARD, P. A. 1956 Airflow over mountains. *Q. J. R. Met. Soc.* **75**, 528–529.
- SMITH, F. T. 1978 The laminar separation of an incompressible fluid streaming past a smooth surface. *Proc. R. Soc. Lond. A* **357**, 443–463.

- SMITH, R. B. 1980 Linear theory of stratified hydrostatic flow past an isolated mountain. *Tellus* **32**, 348–364.
- SMITH, R. B., GLEASON, A. C., GLUHOSKY, P. A. & GRUBISIC, V. 1997 The wake of St Vincent. *J. Atmos. Sci.* **54**, 606–623.
- SMITH, R. B. & GRUBISIC, V. 1993 Aerial observations of Hawaii's wake. *J. Atmos. Sci.* **50**, 3728–3750.
- SMOLARKIEWICZ, P. K., RASMUSSEN, R. M. & CLARK, T. L. 1988 On the dynamics of Hawaiian cloud bands: island forcing. *J. Atmos. Sci.* **13**, 1872–1905.
- SMOLARKIEWICZ, P. K. & ROTUNNO, R. 1989 Low Froude-number flow past 3-dimensional obstacles. Part 1: Baroclinically generated lee vortices. *J. Atmos. Sci.* **46**, 1154–1164.
- SNYDER, W. H., BRITTER, R. & HUNT, J. C. R. 1980 A fluid modeling study of the flow structure and plume impingement on a three-dimensional hill in stably stratified flow. In *Proc. 5th Intl Conf. on Wind Engng* (ed. J. Cermak), pp. 319–329. Pergamon.
- SYCHEV, V. V. 1972 On laminar separation. *Izv. Akad. Nauk SSSR, Mekh. Zhid. i Gaza* **3**, 47–59.
- SYSOeva, E. Y. & CHASHECHKIN, Y. D. 1988 Spatial structure of a wake behind a sphere in a stratified liquid. *J. Appl. Mech. Tech. Phys.* **5**, 655–660.
- VOSPER, S. B., CASTRO, I. P., SNYDER, W. H. & MOBBS, S. D. 1999 Experimental studies of strongly stratified flow past three-dimensional orography. *J. Fluid Mech.* **390**, 223–249.